Damage identification based on response-only measurements using cepstrum analysis and artificial neural networks

Ulrike Dackermann[1*], Wade A. Smith[2] and Robert B. Randall[2]

[1] School of Civil and Environmental Engineering, Faculty of Engineering and Information Technology, University of Technology Sydney, P.O. Box 123, Broadway, NSW 2007, Australia

[2] School of Mechanical and Manufacturing Engineering, Faculty of Engineering, The University of New South Wales, Sydney, Australia

[*] Corresponding author: E-mail: Ulrike.Dackermann@uts.edu.au; Tel.: +61 2 9514 9064; Fax: +61 2 9514 2633

Abstract

This paper presents a response-only structural health monitoring (SHM) technique that utilises cepstrum analysis and artificial neural networks (ANNs) for the identification of damage in civil engineering structures.

The method begins by applying cepstrum-based operational modal analysis (OMA), which separates source and transmission path effects to determine the structure's frequency response functions (FRFs) from response measurements only. Principal component analysis (PCA) is applied to the obtained FRFs to reduce the data size, and structural damage is then detected using a two-stage ensemble of ANNs.

The proposed method is verified both experimentally and numerically using a laboratory two-storey framed structure and a finite element (FE) representation, both subjected to a single

excitation. The laboratory structure is tested on a large-scale shake table generating ambient loading of Gaussian distribution. In the numerical investigation, the same input is applied to the FE model, but the obtained responses are polluted with different levels of white Gaussian noise to better replicate real-life conditions. The damage is simulated in the experimental and numerical investigations by changing the condition of individual joint elements from fixed to pinned. In total, four single joint changes are investigated.

The results of the investigation show that the proposed method is effective in identifying joint damage in a multi-storey structure based on response-only measurements in the presence of a single input. Because the technique does not require a precise knowledge of the excitation, it has the potential for use in online structural health monitoring. Recommendations are given as to how the method could be applied to the more general multiple-input case.

Keywords

structural health monitoring, frequency response function, cepstrum analysis, artificial neural networks, damage identification, principal component analysis, multiple-storey framed structure, operational modal analysis, civil engineering structure

Introduction

The concept of structural health monitoring (SHM) was developed in the 1960s and is applied today by infrastructure owners and authorities to assess the health condition of a structure and to prolong its lifespan. All civil structures have finite lives, and they begin to deteriorate as soon as they are put into service, due to processes such as corrosion, fatigue, erosion, wear and overloading. Thus, early and reliable damage detection and health assessment is critically important to ensure the safety and reliability of ageing structures and to prevent catastrophic failures of essential civil infrastructure.

SHM most commonly employs local and offline assessment techniques, with visual inspection being the most widespread method, followed by local non-destructive testing (NDT) techniques such as stress wave, ultrasonic wave, X-ray, magnetic field, radiography or thermal field methods (1). Most of these practised techniques, however, are very labour intensive and time consuming (2), and often disassembly of secondary parts is required to gain access to vital load-bearing structural elements. Global techniques, on the other hand, monitor the behaviour of the entire structure, which is influenced by local changes, and hence, by solving an inverse problem, they detect, locate and evaluate damage with minimal labour and cost, and without requiring access to the damaged sites. Due to these benefits, during the last two decades, a major focus of SHM research has been to develop global NDT techniques, particularly ones that can be applied remotely and without supervision, thus making them suitable for online SHM applications. As such, vibration-based techniques have received much attention for their effectiveness and practicality (3). Typical vibration-based parameters used for SHM include both indirectly measured data – such as resonant frequencies, mode shapes, modal flexibilities, modal stiffness and modal strain energy – and directly measured data – such as time domain data, power spectral densities and frequency response functions (FRFs) (1). Most developed vibration-based techniques are based on forced impact testing with known excitation forces and indirectly measured response data derived from experimental modal analysis (EMA). The disadvantage of such methods is that they cannot be used for most online SHM as they require precise knowledge of the excitation forces, which typically involves the interruption of operational activities either to measure the applied forces or to apply a known force, and they involve the application of EMA, which is labour intensive and sensitive to human-induced errors. Ambient-vibration-based methods, on the other hand, can operate solely on output-only response signals of a structure, thus making them very attractive for automated online SHM. In these methods, a structure is typically excited naturally by ambient loading from sources

such as traffic, wind, or micro-earthquakes (4). The advantage of using ambient sources is that once a monitoring system is installed, it continuously measures the structural response and records data, without the need for interrupting operations such as traffic flow. A shortcoming of using ambient vibration excitation for SHM and damage detection is, however, that the excitation forces can usually not be measured, and therefore, traditional EMA methods cannot be applied for the identification of modal parameters. Due to this limitation, a large amount of research has been conducted on developing operational modal analysis (OMA) techniques that can extract dynamic characteristics from response-only measurements, and on the application of such techniques to vibration-based damage detection (5-7). Unfortunately, most ambient-vibration-based methods developed to date fail to determine reliable dynamic characteristics and to satisfactorily detect damage in real-life structures. A major challenge in OMA and response-only damage detection is to separate excitation and transmission path effects in response measurements to allow for the determination of relevant structural properties. One way to achieve this source-path separation is with the cepstrum, which is able to deal with 'frequentially smooth' (not just frequentially white) inputs.

Since its original conception in the 1960s for the detection of echoes in seismic time signals (8), the cepstrum has been used in a wide variety of fields, such as audio processing, radar and medical imaging (9). The first use of the cepstrum as a source-path separation tool seems to have been in speech analysis (10), and applications of OMA to simple structures have been researched for many years, with Randall and Gao developing the field throughout the 1990s (11-13). Cepstrum-based OMA works by first isolating the part of the response signal dominated by transmission path effects and then, via a curve-fitting approach, obtaining the poles and zeros of the transfer function, from which the system's FRFs can be generated. Randall and Gao used this approach on a simple steel beam, and they showed that very accurate FRFs could be determined from response-only measurements (11-13). Since the derived FRFs

are sensitive to structural changes, they contain damage-relevant information and can thus be used to detect damage. While cepstral source-path separation techniques have been used on some mechanical structures (14, 15) and on a simple steel beam, their use for online SHM of civil structures remains unexplored.

The use of FRFs derived from forced impact testing with known excitation forces, on the other hand, has been investigated for the damage detection and SHM of civil structures for the past two decades by several researchers. Choudhury and He (16) presented a method to locate damage based on directly measured FRF data from impact testing. The researchers introduced a Damage Location Vector (DLV) that is calculated using FRF measurements from the damaged system and an undamaged model. The damage is located by applying dynamic expansion methods. The method was successfully verified by a numerical and an experimental study on a frame structure. The researchers Sampaio, Maia and Silva (17) proposed to use FRF curvature data for damage detection. Their presented method was an extension of the Mode Shape Curvature Method by Pandey et al. (18) and uses absolute differences in FRF curvatures between the undamaged and damaged states of a structure obtained from forced impact testing. The researchers validated the method with a numerical study of a lumped-mass system and an experimental study using data from a real bridge (the I-40 bridge over the Rio Grande in New Mexico). They showed that their FRF-based method performs well in detecting and locating damage, even in the presence of noise. It was however reiterated that the method required further development for better damage quantification. Ni, Zhou and Ko (19) presented an experimental investigation of seismic damage identification of a 38-storey building model using FRFs, Principal Component Analysis (PCA) and neural networks. A 1:20 scale reinforced concrete structure was tested on a shake table by exerting successively enhanced ground earthquake excitations to generate different levels of damage. PCA was performed on the measured FRFs to reduce their dimension and to eliminate noise, and the compressed FRF

data were subsequently used as inputs to neural networks. The results demonstrated that, provided a sufficient sensor distribution is employed, a quite satisfactory evaluation and localisation of damage is obtained. The authors further found that compared to the direct FRF method, the PCA-compressed FRF method provided much higher identification accuracy in assessing the damage.

This paper aims to address the gap between using FRFs obtained from forced impact testing with known excitation forces, and FRF data obtained from ambient vibration excitation with response-only measurements. The paper proposes the use of cepstrum-based OMA to determine FRFs for use as damage indices for the identification of damage in structures based on response-only measurements. The proposed technique is applied to a two-storey framed structure with various cases of joint damage. PCA and neural network ensemble techniques are used to extract damage features in the cepstrum-based FRFs and to identify the damage. To enhance embedded damage features in the derived FRFs, residual FRFs, which are differences in FRFs between the undamaged and the damaged structure, are determined. PCA techniques are employed to compress residual FRFs to a few principal components (PCs) to generate suitable input data for neural network training and damage detection. In order to analyse measurements obtained from different locations, an innovative two-stage hierarchical system of artificial neural network (ANN) ensembles is trained to evaluate damage patterns in the PC data. The proposed method is verified on both experimental and numerical models of the two-storey framed structure. Joint damage is simulated by changing the condition of individual joint elements of the structure from fixed to pinned. To consider real life applications and to investigate the robustness of the method to noise, the ambient vibration responses obtained from the numerical model are polluted with different levels of white Gaussian noise up to 10% noise-to-signal ratio.

In a previous study conducted by the lead author, a similar damage detection algorithm based on FRFs, PCA and network ensembles was successfully applied to a numerical and experimental two-storey framed structure under forced impact excitation. From this investigation, it was found that the proposed damage detection algorithm was capable of accurately and reliably detecting damage from forced impact loading (20, 21). The method is now extended in this study to damage detection with ambient vibration excitation, increasing its potential for application in continuous online SHM. A recent paper by the authors presents more details on the numerical investigation using response-only measurements (22).

Background on cepstrum-based operational modal analysis

Operational modal analysis

This paper makes use of operational modal analysis, which differs from the more widely-known experimental modal analysis in two important respects. Both techniques involve the experimental determination of a structure's dynamic characteristics (e.g. resonances, damping and mode shapes), but unlike EMA, OMA is:

- based on response-only measurements, without precise knowledge of the excitation forces acting on the structure;
- generally employed *in operation*, where the structure is subjected to real-life operating forces and conditions, rather than a laboratory environment.

While OMA possesses a number of advantages over EMA, its reliance on response-only measurements requires different techniques in order to extract modal properties (23). Response measurements, of course, typically comprise both excitation and transmission path effects, and these need to be separated before the structural properties can be determined. Most established OMA techniques achieve this source-path separation by assuming the excitation to be

frequentially white (24), but the cepstrum-based method employed in this paper relaxes that requirement, as discussed further in the following sections.

The cepstrum

Various definitions for the cepstrum exist (25); here we shall use the so-called 'real cepstrum', defined for a time signal $x(t)$ as:

$$\hat{x}(\tau) = F^{-1}\left[\log\left(\left|X\left(f\right)\right|\right)\right] \tag{1}$$

and the 'complex cepstrum' as:

$$\hat{x}_c(\tau) = F^{-1}\left[\log\left(X\left(f\right)\right)\right] \tag{2}$$

where $X(f)=F[x(t)]$ is the (complex-valued) Fourier transform of $x(t)$. Table 1 includes a number of terms often employed when using the cepstrum.

Table 1 Cepstrum terminology

Frequency domain	Cepstrum domain
Frequency	Quefrency
Spectrum	Cepstrum
Filtering	Liftering
High-pass filter	Long-pass lifter

Note that, being real-valued, the real cepstrum includes no phase information, so the original time signal is not recoverable after liftering in the cepstrum domain. However, the process from the amplitude spectrum to the real cepstrum is reversible, and so the amplitude spectrum can be obtained after cepstral editing (26), as exploited in this paper. The 'complex' cepstrum here is also real-valued, includes phase information, and is thus fully invertible, i.e., $x(t)$ can be recovered after liftering the cepstrum.

Source-path separation

For a linear time-invariant (LTI) system subjected to a single input $x(t)$, the system response $y(t)$ is the convolution of the input and the impulse response function $h(t)$, i.e.:

$$y(t) = h(t) * x(t) = \int_{-\infty}^{\infty} h(t) \cdot x(t-\tau) \cdot d\tau \tag{3}$$

In the frequency domain, expressing the relationship in terms of the complex spectra (or Fourier transforms of the time records), the convolution becomes multiplicative:

$$Y(f) = H(f) \cdot X(f) \tag{4}$$

in which $H(f)$ is the FRF. For the real cepstrum the respective moduli can be used. Taking the log and the inverse Fourier transform, we obtain the cepstra, in which source and path effects are additive:

$$\hat{y}(\tau) = \hat{h}(\tau) + \hat{x}(\tau) \quad \text{and} \quad \hat{y}_c(\tau) = \hat{h}_c(\tau) + \hat{x}_c(\tau) \tag{5}$$

Thus in circumstances in which the input occupies defined regions of the cepstrum, the source effects can easily be separated (via appropriate liftering) from those of the transmission path, which usually occupy a broader quefrency range. Examples of such inputs include frequentially smooth and flat forces, which are concentrated in the low quefrency region, such as a hammer blow, which does not have to be white (13). The working assumption of this study is that the ambient excitation of many structures would also satisfy this criterion. These types of inputs can be removed from the response cepstrum via long-pass liftering, leaving only the path cepstrum, from which the system's FRF can be recovered. It should be noted that this is a much less restrictive requirement than the common white noise input assumption made by most other blind source-path separation techniques.

The FRF obtained directly from the path cepstrum would generally contain considerable noise, but there exists an analytical relationship between the path complex cepstrum $\hat{h}_c$ and the

transfer function's poles and zeros, and this relationship can be used to curve-fit the path cepstrum to obtain the poles and zeros, from which the FRF can be regenerated to within a scaling factor.

For a sampled sequence, the transfer function of (4) can be expressed in the z-plane as:

$$H(z)=\frac{Bz^{r}\prod_{k=1}^{N_{zi}}\left(1-a_{k}z^{-1}\right)\prod_{k=1}^{N_{zo}}\left(1-b_{k}z\right)}{\prod_{k=1}^{N_{pi}}\left(1-c_{k}z^{-1}\right)\prod_{k=1}^{N_{po}}\left(1-d_{k}z\right)} \tag{6}$$

where a_k and c_k represent the zeros and poles inside the unit circle, and b_k and d_k the zeros and poles outside the unit circle, respectively (where $|a_k|,|b_k|,|c_k|,|d_k|<1$). A stable minimum phase system (applies to many simple structures), however, contains only poles and zeros inside the unit circle, and, based on a more general expression by Oppenheim and Schafer (27), Gao and Randall (12) showed that for such systems the complex cepstrum corresponding to $H(z)$ can be expressed in terms of these poles and zeros:

$$\hat{h}_{c}(n)=\begin{cases}\log|B| & n=0\\ 2\sum_{k=1}^{N_{pi}/2}\frac{A_{ck}^{n}}{n}\cos\left(\omega_{ck}n\right)-2\sum_{k=1}^{N_{zi}/2}\frac{A_{ak}^{n}}{n}\cos\left(\omega_{ak}n\right) & n>0\\ 0 & n<0\end{cases} \tag{7}$$

in which n is the quefrency index and where, for example, a pair of poles, c_k, is represented by $(2/n)\,A_{ck}^{n}\cos(\omega_{ck}n)$ in which $A_{ck}=|c_k|$ and $\omega_{ck}=\angle c_k$ represent, for each pole, the damping and the damped natural frequency, respectively, and likewise for the zeros a_k. Oppenheim and Schafer (27) showed that for a minimum phase system, the complex cepstrum $\hat{h}_c(n)$ in (7) can be obtained from the two-sided real cepstrum, derived from the log amplitude spectrum only, by doubling its positive quefrency components and setting its negative quefrency components to zero. This has the advantage that, since only the spectrum amplitude is required, the response spectrum can be averaged (with Welch's method, for example) to remove noise, and the phase

does not have to be unwrapped. (Implicit in the above is that the Fourier transforms of (1) and (2) have been replaced by z-transforms in the calculation of the cepstrum.)

Thus, according to the above, by curve-fitting a liftered form of the response cepstrum (to remove source effects), one can obtain the transfer function's poles and zeros, from which the FRF can be regenerated to within a scaling factor (since B in (6) is not recovered from the curve-fitting process). However, the obtained FRF will be subject to magnitude distortion associated with truncation. This results from the use of an incomplete pole-zero model to represent the transfer function. Such models produce FRFs with the correct locations of poles and zeros in the considered frequency band, but are subject to the effects of out-of-band poles and zeros, which manifest as a distortion of the general slope of the regenerated FRFs. A number of techniques have been developed to overcome this distortion (28); in this study, however, the FRF scaling (both absolute and relative) is not critical as the proposed method is applied to a structure excited by a force with specified frequency characteristics that remain unchanged from test to test (discussed in the following sections). As such, unprocessed regenerated FRFs are used as damage indices, without the need for scaling or magnitude correction.

It should be noted that the above arguments apply to single-input-multiple-output (SIMO) systems only, and a real-life structure would generally not strictly satisfy that requirement. The response of a multiple-input-multiple-output (MIMO) system is given by a sum of convolutions, which cannot easily be separated. In the frequency domain, the sum of convolutions becomes a sum of ratios of polynomials, of which the denominators are all the same. The summed numerator is another polynomial whose roots represent the zeros of the MIMO response. In other words, the contributions of the various inputs to the response of a particular point in a MIMO system are such that the poles will reinforce while the zeros, in general, will not. This means that the zeros of a MIMO response are dependent on the force

distribution, so while they may contain information about structural condition, they could not be used for comparison unless the force distribution remained unchanged – a requirement that would be difficult to satisfy in many practical applications. This could perhaps be negated in practice by curve-fitting only the poles and not the zeros, the idea being that the system's poles are where a great deal of structure-state information is likely to reside. This idea, however, is not explored further in this paper since the focus is a simplified SIMO structure, as explained in the following section.

Test structure

The proposed cepstrum-based damage identification method was validated on an experimental and a corresponding finite element (FE) model of a two-storey framed structure. The experimental structure was manufactured and tested in the Structures Laboratory of the University of Technology Sydney (UTS). To simulate ambient vibration, the structure was dynamically tested using a 3 × 3 m shake table with random white noise excitation. The matching numerical structure was modelled with the software ANSYS using transient analysis to simulate ambient excitation. Various cases of joint damage were simulated in the experimental and FE structures by changing the condition of connection joints from fixed to pinned. The structures used in the laboratory and numerical investigations are depicted in Figure 1 and Figure 3, respectively.

Experimental investigation

The experimental model of the two-storey framed structure consisted of two columns, two crossbeams and four joint elements. The structure had an overall dimension of 1,600 × 800 mm. The two columns were made of flat steel and had a cross-section of 65 × 5.5 mm and a height of 1,600 mm. They were mounted 800 mm apart to a base platform with two steel angles each

creating a fixed connection. The two crossbeams were specially designed to allow an exchange of the joint elements (either fully pinned or fully fixed). The crossbeams consisted of a box section of 150 × 50 mm and were located at heights of 700 mm and 1,400 mm above the base connection. The steel had a modulus of elasticity of 200×10^9 N/m^2, a Poisson's ratio of 0.3 and a density of 7,850 kg/m^3. The entire structure had a mass of approximately 87 kg. A photo of the structure displaying relevant dimensions and structural elements is shown in Figure 1 (a).

To generate different data for appropriate generalised neural network training and testing, the experimental investigation was conducted with the structure in two different states. In the first state, the two columns were undamaged and in the second state, one of the columns was exchange with a damaged column, which had a cut with a width of 4 mm and a depth of 32.5 mm (see insert in Figure 1 (b)). Thereby, data from two structures, which are structurally similar but not the same, are generated. Both structures were tested on a shake table with different joint damage scenarios and acceleration response data was recorded from ambient vibration excitation. In the data post-processing, the data from the structure with the undamaged column was used to train the neural networks, while the data from the structure with the damaged column was used to validate and test the networks with hitherto unseen data. Such an approach does not only test the recall ability of networks but provides a generalised validation of the proposed method with two unrelated data sets being used for network training and testing.

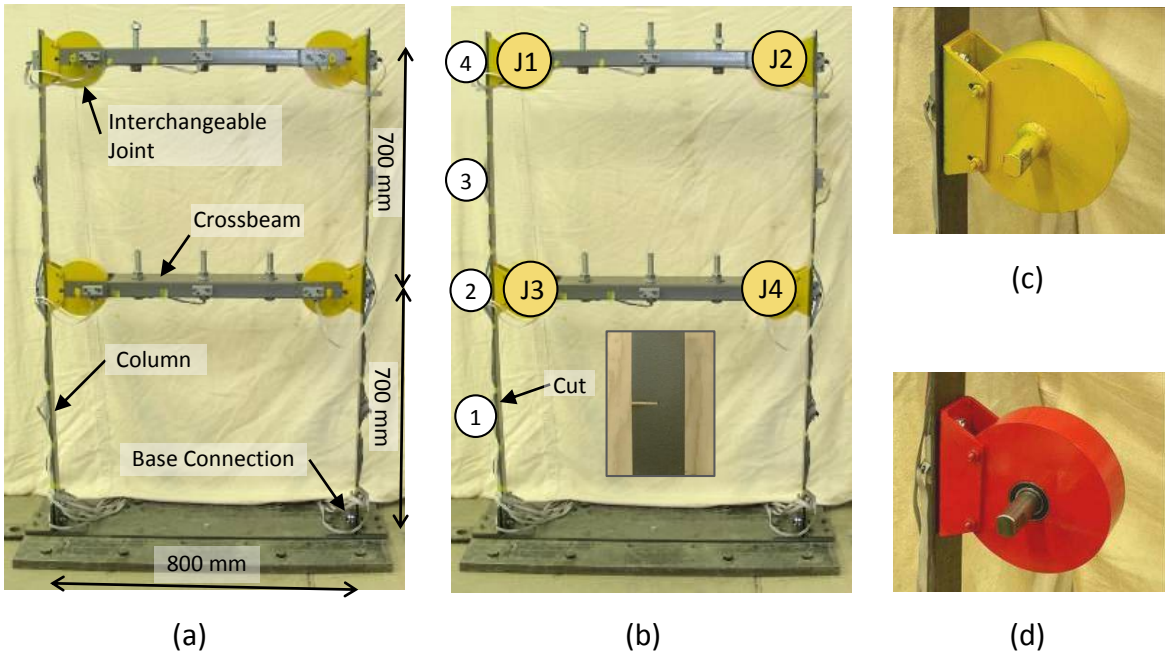

Figure 1. Experimental two-storey framed structure. (a) Structural elements and relevant dimensions, (b) accelerometer locations (1 to 4) and interchangeable joints (J1 to J4), (c) fixed joint and (d) pinned joint.

To simulate joint damage, the four joint elements (J1 to J4, see Figure 1 (b)) that connect the crossbeams with the columns were interchangeable from fully pinned to fully fixed. In practice, joint changes are generally caused by environmental or ageing decay, such as corrosion or loosening of connections, and are a common and serious issue in aged civil engineering structures. For the fixed joint element, the shaft (shown in Figure 1 (c)) was welded to the body of the joint, providing a rigid connection. For the pinned joint element, a roller bearing was installed on the shaft, allowing the pin to rotate freely (see Figure 1 (c)). As the undamaged state of the structure, the four connections were all fixed joint elements (termed FFFF). Four scenarios of single joint changes were studied by replacing, one at a time, the four fixed joints with a pinned joint. For both structural states (with and without column damage), five different joint scenarios were investigated, as listed in Table 2.

Table 2. Investigated joint scenarios

Joint scenario	Damage state	Joint condition			
		J1	J2	J3	J4
FFFF	undamaged	F	F	F	F
PFFF	damaged	P	F	F	F
FPFF	damaged	F	P	F	F
FFPF	damaged	F	F	P	F
FFFP	damaged	F	F	F	P

Note: F indicates a fixed joint and P a pinned joint

To simulate ambient excitation, the structure was dynamically tested using a 3 × 3 m shake table. The unidirectional shake table facility at UTS can move in the horizontal direction via a hydraulic actuator with a maximum acceleration of 25 m/s^2 (bare table), and a maximum stroke and piston velocity of ±100 mm and 550 mm/s, respectively. The structure was firmly mounted to the shake table and subjected to a random acceleration of Gaussian distribution, with a mean of 0 and a standard deviation of 0.07 m/s^2. The acceleration time history of the excitation force is displayed in Figure 2 (a) along with its frequency spectrum in Figure 2 (b). For each investigated joint scenario, the structure was excited with the random loading for a duration of 600 s.

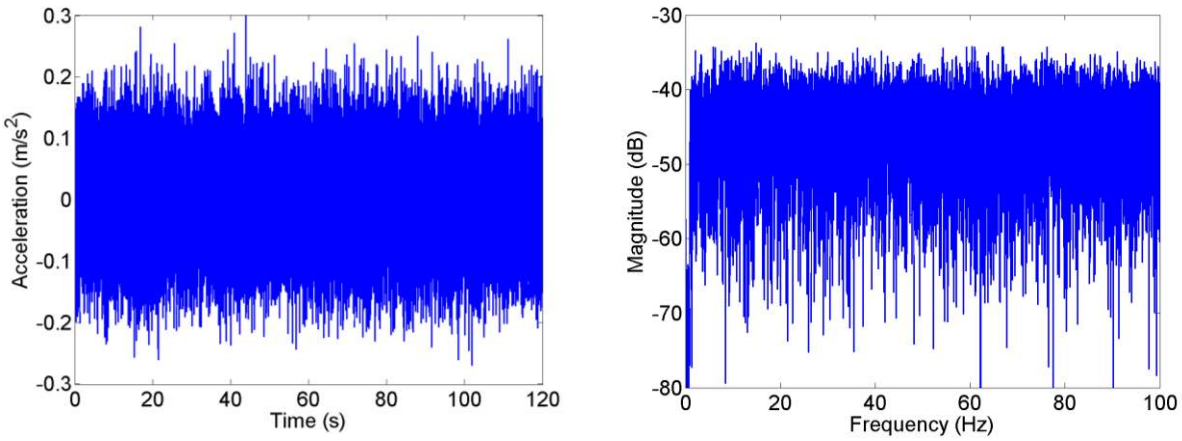

(a) (b)

Figure 2. Ambient white Gaussian noise excitation, (a) acceleration time history and (b) frequency spectrum.

For the duration of the excitation, the horizontal responses of the structure were measured with accelerometers along one of the columns at measurement locations '1' to '4', as indicated in Figure 1 (b). The sensors used were piezoelectric accelerometers of PCB model 352C34, having a sensitivity of 100 mV/g with a frequency range of 0.5 Hz to 10,000 Hz. The acquired time history signals were amplified and conditioned by a multi-channel signal conditioner (PCB model 483B03). For each test, the sampling rate was set to 400 Hz with a testing duration of 600 s, thus capturing 240,000 data points per test. Since it was desirable for ANN training to capture as many data sets as possible, the acceleration measurements were equally divided into five different sets to simulate five individual tests. Accordingly, the data of the divided acceleration time histories comprised a time record of 120 s and 48,000 data points. In total, for each structural state (with and without column damage), 25 data sets were recorded (5 joint scenarios × 5 data sets). The natural frequencies of the first seven modes of the undamaged state (without column damage and with four fixed joints) were determined for the experimental structure as 2.26 Hz, 6.89 Hz, 67.03 Hz, 67.03 Hz, 82.10 Hz, 98.90 Hz and 115.39 Hz.

Numerical investigation

The numerical model of the two-storey framed structure was created according to the dimensions and material properties of the experimental structure using the FE software ANSYS. First, the main bodies of the structure (i.e. column, crossbeam, joint element and base connection) were generated and then the individual bodies were connected by defining the contact regions. SOLID187 was used as the element type, which is a tetrahedral structural solid defined by ten nodes having three degrees of freedom at each node (i.e. translations in the nodal x, y and z directions). For the modelling of a fixed joint element (undamaged condition), the contact region between crossbeam and joint element was made rigid, as depicted in Figure 3 (c)). For the pinned connection (damaged condition), the rigid contact region was replaced by a revolute joint connection (Figure 3 (d)). The revolute joint was constrained in five local degrees of freedom (UX, UY, UZ, ROTX, ROTY) and free in ROTZ, which allows free rotation around the z-axis. As with the experimental investigation, the structure was modelled in the undamaged state (with four fixed joints) and with four different joint damage scenarios where, in turn, each of the four fixed joints was replaced with a pinned revolute joint.

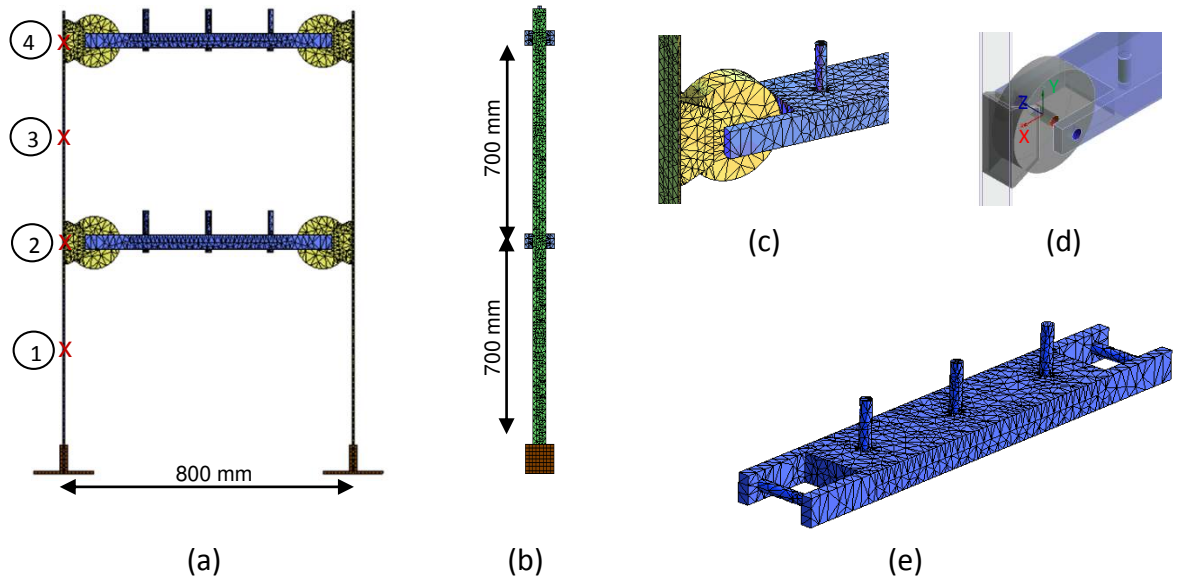

Figure 3. Numerical two-storey framed structure (a) front view, (b) side view, (c) fixed joint element, (d) revolute joint connection and (e) crossbeam.

For the ambient excitation, the undamaged and damaged models were subjected to white Gaussian noise loading using transient analysis in ANSYS Classic. As with the experimental testing, a random acceleration of Gaussian distribution, with a mean of 0 and a standard deviation of 0.07 m/s^2, was applied in the horizontal direction to the base of the structure. The ambient loading was applied for 600 s with integration time steps of 0.0025 s for a sampling frequency of 400 Hz. The horizontal displacement responses of the structure were recorded at the same locations ('1' to '4', as indicated with crosses in Figure 3 (a)). From the displacement responses, acceleration data was obtained by double differentiation. To simulate real testing conditions and to generate different data sets for network training, the acceleration time histories were polluted with white Gaussian noise to simulate measurement noise interference experienced during experimental testing. In total, noise of four intensities (1%, 2%, 5% and 10% noise-to-signal ratio) was added to the acceleration response time histories. As with the experimental data, the response time histories were divided into five sets of 120 s recording time each, giving a total of 100 data sets (5 joint scenarios × 5 data sets × 4 levels of noise

pollution). Since noise pollution of up to 10% noise-to-signal ratio already generates large data variations, it was not necessary for appropriate generalised neural network testing to introduce an additional structural state where a column was inflicted with damage. The natural frequencies of the first seven modes of the undamaged state (without column damage and with four fixed joints) were determined for the numerical model as 2.23 Hz, 6.50 Hz, 66.07 Hz, 72.56 Hz, 90.20 Hz, 101.53 Hz and 130.30 Hz.

Methodology

Cepstrum analysis

The previously-described cepstrum-based OMA theory was applied to the acquired data from the experimental and the finite element structure using MATLAB. First, the PSDs of the system response measurements were determined, from which estimates of the resonances and anti-resonances were specified and used as initial values in the complex cepstrum curve-fitting process. Before curve-fitting, a rectangular long-pass lifter was applied to the response cepstrum, leaving that portion of the cepstrum dominated by transmission path effects. The FRFs were then regenerated by adding (in log amplitude) the individual contributions from the obtained poles and zeros. Note that because the input was white, the liftering process was not strictly required here, as the input would be (theoretically) represented by only the zero-quefrency component, which defines only the absolute scaling. In practical applications, of course, liftering would generally be required because the colour of the input would not be constant.

An example of a PSD and the corresponding cepstrum-based FRF from the undamaged laboratory structure are shown in Figure 4. Some amplitude distortion of the cepstrum-based

FRF can be seen in the plot, a result of the truncation of out-of-band poles and zeros. Nevertheless, it is clear that the cepstrum FRF represents the measurements very well.

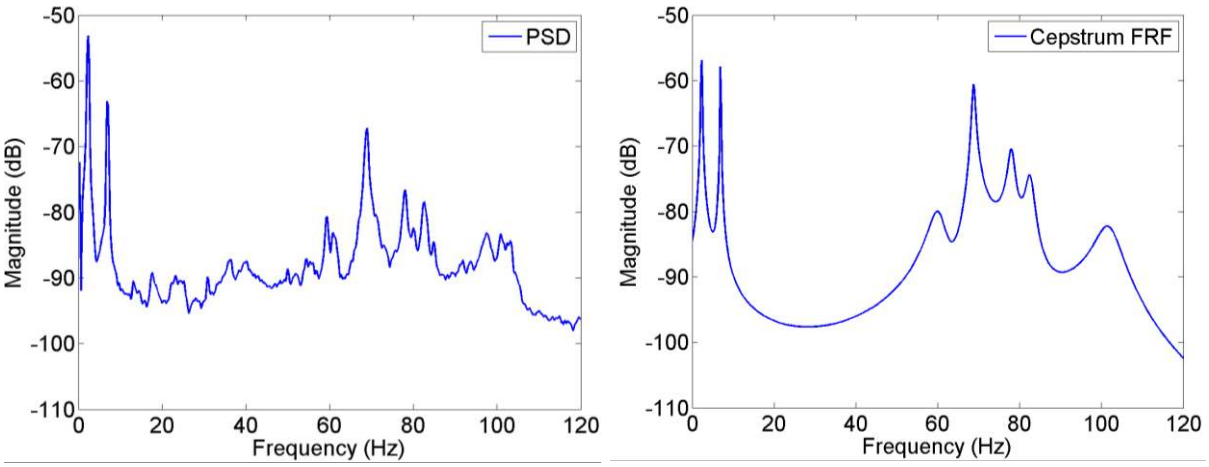

(a) (b)

Figure 4. (a) PSD and (b) cepstrum-derived FRF of the undamaged laboratory structure (FFFF) from averaged measurement points '1' to '4'.

Residual FRFs

For illustration, the cepstrum-derived FRFs of the finite element structure in the undamaged case and four joint-damaged cases are shown in Figure 5 (a). From the displayed figure, it can be seen that the FRFs are quite distinct from one another. Resonant peaks not only shift or change amplitude, the different FRFs show completely new patterns with some new resonant peaks emerging and others disappearing. These changes of the resonant peaks in the FRFs reflect changes in the vibrational modes of the structure and can be used to detect damage.

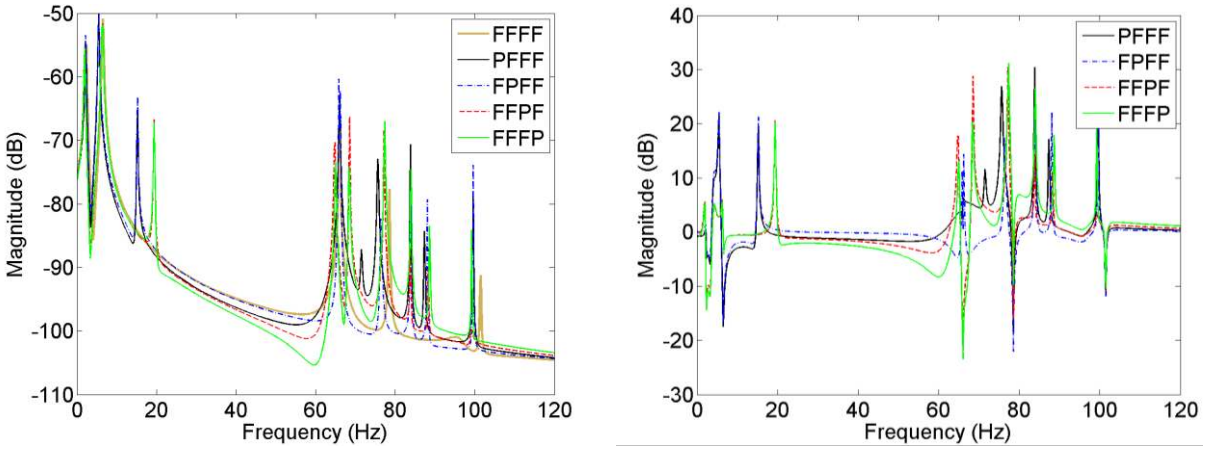

(a) (b)

Figure 5. (a) Cepstrum-derived FRFs of undamaged and damaged cases, and (b) residual FRFs of damaged cases. Displayed are data from measurement point '2' of 1% noise pollution.

To extract and enhance the damage patterns embedded in the cepstrum-derived FRF data, the proposed method uses residual FRFs, which are differences in FRF data (in log amplitude) between the undamaged and the damaged structure. Residual FRFs are defined in Equation (8), with $H_d(\omega)$ being the FRF data from the damaged structure and $H_{und}(\omega)$ being the FRF data from the undamaged structure.

$$ResH(\omega) = \log\left[\left|H_d(\omega)\right|\right] - \log\left[\left|H_{und}(\omega)\right|\right] \tag{8}$$

The corresponding residual FRFs of the cepstrum-derived FRFs displayed in Figure 5 (a) are shown in Figure 5 (b). From the figure, it is noted that residual FRF values closest to the frequency peaks are most affected by the damage. These unique patterns in residual FRFs were subsequently used to identify the damage.

Principal component transformation

To produce input parameters that are suitable for ANN training and to further extract relevant damage features in the residual FRFs, the application of Principal Component Analysis (PCA)

is proposed in this study. The full-size residual FRF contained 1,025 spectral lines and covered a frequency range of 0 to 200 Hz. This corresponds to 1,025 input nodes in the neural network, which would cause severe problems in training convergence in addition to computational inefficiency. Therefore, the use of PCA is proposed to reduce the size of the residual FRFs as well as to extract damage patterns.

PCA was developed by Pearson (29) and is one of the most powerful statistical multivariate data analysis techniques for achieving dimensionality reduction. It is a statistical technique that linearly transforms an original set of k variables into a smaller set of n ($n \leq k$) uncorrelated variables, the so-called principal components (PCs). Eigenvalue decomposition of the covariance matrix forms the basis of PCA. The direction of the resulting eigenvectors represents the direction of the PCs, which are weighted according to value of the corresponding eigenvalues. Each PC is a linear combination of the original variables. All the PCs are orthogonal to each other and form an orthogonal basis for the space of the data. The full set of PCs is equal to the original set of variables. By removing PCs of low power, a dimensional reduction is achieved without significantly affecting the original data (30). Besides the benefit of data reduction, PCA is also a powerful tool for disregarding unwanted measurement noise. As noise is a random feature not correlated with a global characteristic of the data set, it is represented by less significant PCs. Therefore, by disregarding PCs of low power, measurement noise is filtered out.

In this study, for the PC transformation, individual matrices were formed from the data of each measurement point as well as averaged data (calculated by averaging the FRFs of measurement locations ‘1’ to ‘4’). The individual matrices contained all residual FRFs of all joint damage scenarios and all noise pollution levels. While the columns of the individual matrices were formed from the 1,025 spectral lines of the residual FRFs, the rows were assembled from the available data sets; i.e. 200 data sets for the laboratory investigation (4

joint damage scenarios × 5 damaged joint data sets × 5 undamaged joint data sets × 2 column damage states), and 400 data sets for the finite element investigation (4 joint damage scenarios × 5 damaged joint data sets × 5 undamaged joint data sets × 4 levels of noise pollution). After PCA transformation, the 1,025 spectral lines of the residual FRFs were projected onto their 1,025 PCs. To reduce the size of the PCA-transformed reduced residual FRFs, the most dominant PCs containing sufficient information to allow the identification of damage had to be determined, so the PCs of higher power were plotted for visual evaluation. As examples, Figure 6 (a) and (b) display the first 15 PCs of the four joint damage scenarios from the experimental investigation (from measurement point '3' and the undamaged column state) and the numerical investigation (from measurement point '2' with 1% noise pollution), respectively. For each depicted scenario, three different data sets are displayed, each generated from a different time window in the response history. From the figures, it can be seen that for both the laboratory and the numerical investigation, the first four PCs show the most distinguishable patterns for the different joint damage scenarios. Also, for each joint damage scenario, the three data sets are grouped together, and thus they are represented by the same/similar PCs. Such clustering behaviour and the distinct PC patterns of the different joint configurations are ideal conditions for neural network based pattern recognition. From these findings, it was concluded that it was sufficient to use the first four PCs as input parameters for the ANN training.

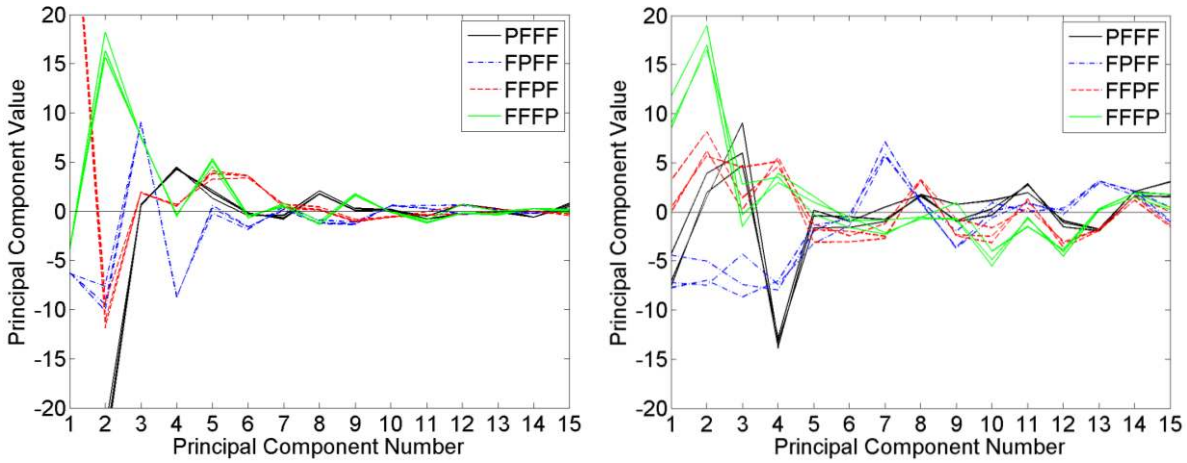

Figure 6. Principal components of residual FRFs of the four investigated joint damage cases for (a) the laboratory investigation (from measurement point '3' and the undamaged column state) and (b) the numerical investigation (from measurement point '2' with 1% noise pollution).

Artificial neural network design

For the laboratory and numerical investigations, a hierarchy of multi-layer back propagation neural networks was created to extract damage patterns from the derived PCA-transformed residual FRFs. For each type of data set (experimental and numerical), five individual networks and one network ensemble (fusing the outcomes of the individual networks) were designed. The five individual networks were trained with the first four PCs of residual FRFs. Four of the five individual networks were fed with data obtained from the four measurement locations ('1' to '4') and one was fed with the data of averaged FRFs from locations '1' to '4'. The network ensemble was trained with the outcomes of the four individual measurement location networks. The results of the individual averaged network were then compared against the results of the neural network ensemble to demonstrate the advantage of the network ensemble. The transfer functions used for all networks were hyperbolic tangent sigmoid functions. As a convergence

algorithm, the conjugate gradient descent function was employed for all networks. The individual neural networks were designed with an input layer of four nodes, representing the number of selected PCs, and two hidden layers of six and five nodes. The network ensemble comprised 16 input nodes, which were the outputs of the four individual measurement location networks, and three hidden layers consisting of 12, 9 and 6 nodes. For the network outcomes, all networks were designed to categorise the conditions of the four joint elements as either fixed or pinned in a winner-takes-all fashion. As such, the network outputs comprised four output nodes. For example, the desired network output for joint condition PFFF was (1,0,0,0). The design of the two-stage neural network ensemble system is displayed in Figure 7.

Figure 7. Design of two-stage neural network ensemble system.

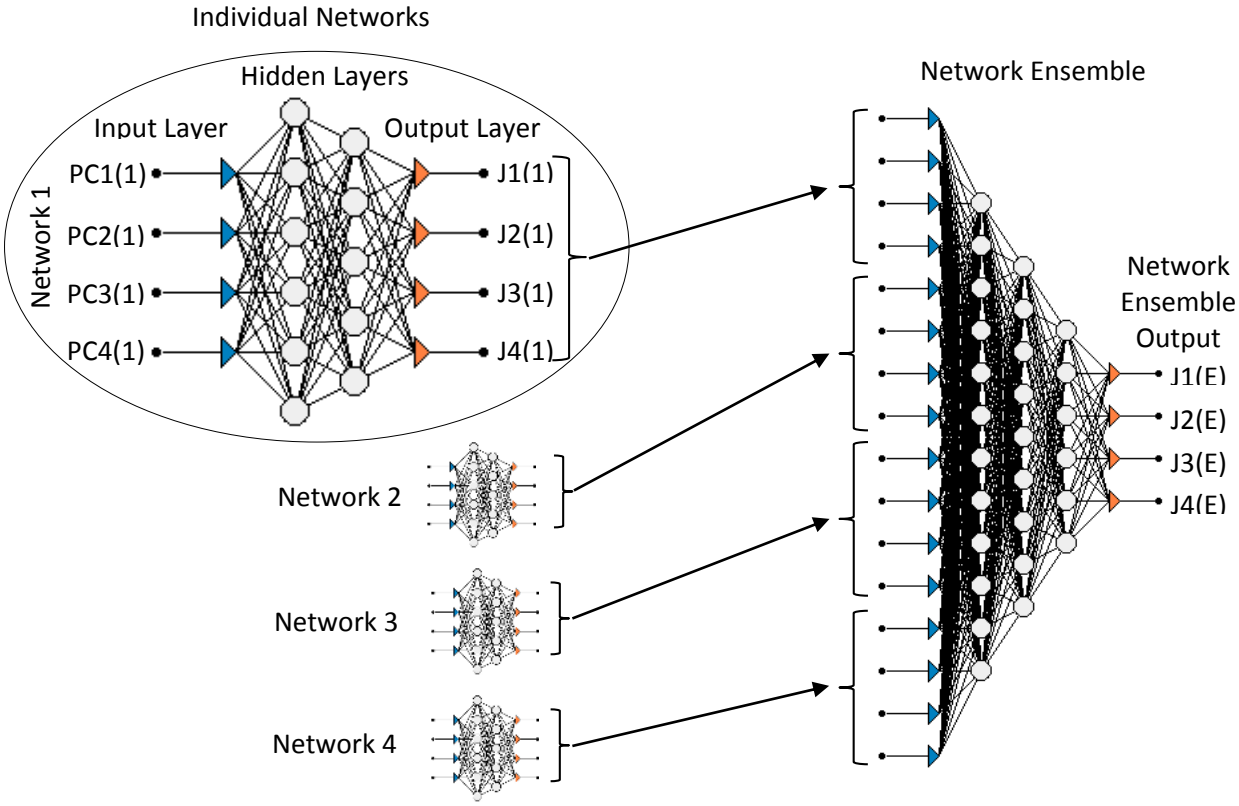

To avoid over fitting and to achieve generalisation, the input data was separated into training, validation and testing sets. While the network was trained with the training samples, its performance was supervised utilising the validation set to avoid over fitting. For the laboratory data, the full set of 100 samples of the structure with no column damage was used to train the

networks, while the set of 100 samples of the structure with column damage was divided into 40 samples for validation and 60 for testing. For the numerical data, the 400 available samples were divided into a set of 240 samples for training and two sets of 80 samples for validation and testing. The data of the different noise pollution levels was equally divided among the training, validation and testing sets. The design and operation of all neural networks was performed with the software Alyuda NeuroIntelligence version 2.2 from Alyuda Research Inc (31).

Process summary and implementation

The proposed methodology is summarised in the flow chart in Figure 8. It should be noted that the process has the potential for automated implementation. However, this would require, in general, dealing with multiple-input cases (discussed previously), and also resolving practical issues such as determining the optimal number of principle components to use and developing an automated pole/zero search algorithm. Yet these practical issues hardly seem insurmountable.

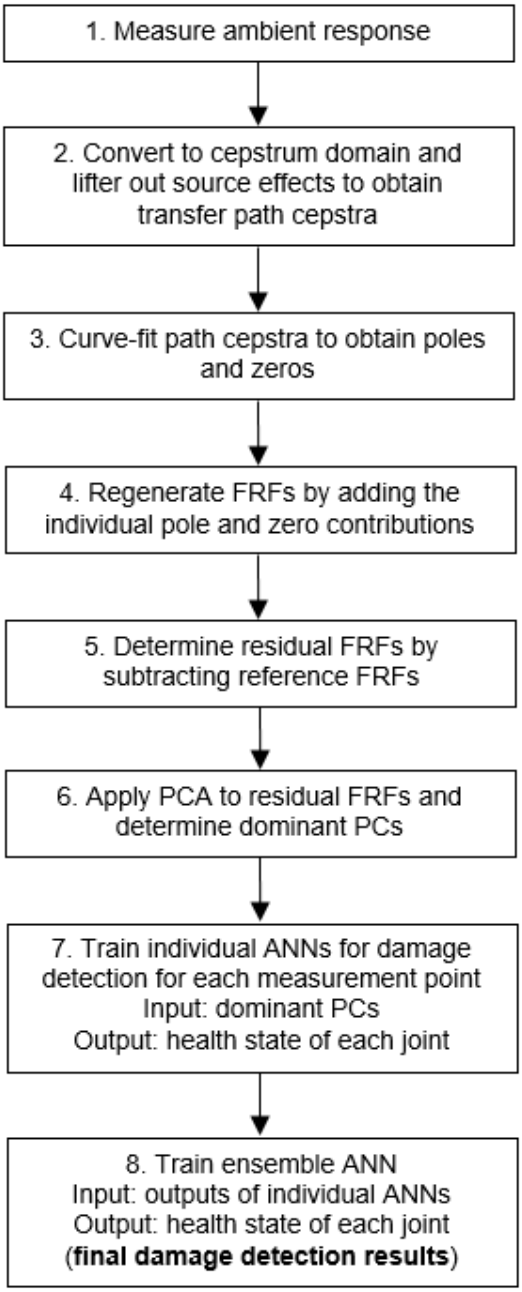

Figure 8. Process summary for proposed methodology.

Results and discussions

This section discusses the results of the proposed method applied to data from both the experimental and finite element investigations. The neural network outcomes for damage identification are presented in two tables and figures. The tables list the network performance of all trained networks; i.e. four individual neural networks trained with FRF data from

measurement locations ‘1’ to ‘4’; one averaged neural network (‘Avg’) and one network ensemble (‘Ens’). The performance is given for the training, validation and testing sets in mean correct classification rate error (MCCRE), which is defined as the number of incorrectly predicted cases normalised by the total number of cases per set. The presented figures illustrate the network performance of the testing set outcomes subdivided by either joint damage scenarios (for experimental investigation), or by the four noise pollution levels (for numerical investigation).

Note that both the tables and the figures from the experimental and numerical investigations are not exactly equivalent and so should not be compared directly. In the case of the tables, the MCCRE values for the numerical investigation are based on all noise levels, some of which clearly overestimate the level of noise in the laboratory data. These noise levels are included to test the method rather than to replicate exactly the laboratory findings. The figures, on the other hand, display different features; one shows the MCCRE of the experimental investigation as a function of the damage type, while the other shows the MCCRE of the numerical investigation as a function of the noise level.

Results of the experimental investigation

For the experimental investigation, the outcome performance of all trained neural networks is listed in Table 3. From the table, it can be seen that for the training set, the networks precisely predicted all studied damage cases. For the validation and testing sets, errors of under 8% were achieved, with the network of location ‘2’ even giving 0% error. While the averaged network produced results that were worse than the best individual network (i.e. network ‘2’), the ensemble network, which fuses the outcomes of all individual measurement location networks, achieved outstanding results with correct predictions for all investigated joint damage cases.

Table 3. Network performance of training, validation and testing sets (in MCCRE [%]) of networks trained with data from the experimental investigation.

Network	'1'	'2'	'3'	'4'	Avg	Ens
Training performance	0.00	0.00	0.00	0.00	0.00	0.00
Validation performance	2.50	0.00	7.50	5.00	2.50	0.00
Testing performance	1.67	0.00	5.00	3.33	1.67	0.00

For closer inspection of the testing set outcomes, Figure 9 displays the results of the testing samples subdivided by joint damage scenarios. From the figure it can be observed that the false predictions are across all four investigated joint damage scenarios, which indicates that there is no bias in the investigated joint damage cases. Network '3' obtained the poorest outcomes, with two wrong estimations for case 'FPFF' and one wrong estimation for case 'PFFF' (out of 15 testing samples for each joint damage scenario).

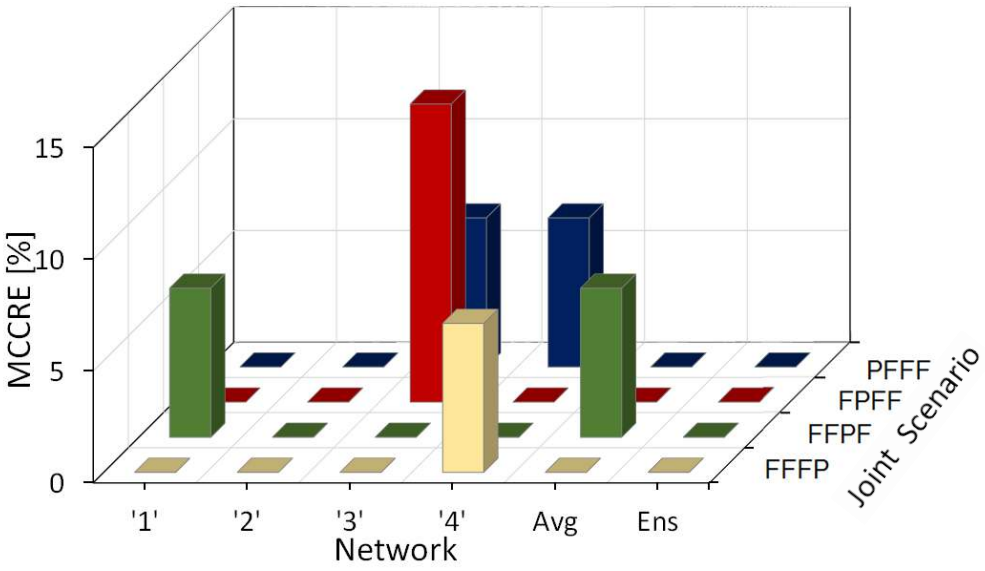

Figure 9. Network performance of laboratory investigation with column damage subdivided by joint damage scenario (testing data set).

Results of the numerical investigation

For the numerical investigation, the network results are listed in Table 4. The results are generally poorer than the outcomes of the experimental study, due to noise contamination of up to 10%, which is significantly larger than the noise level experienced in laboratory testing. The obtained neural network errors are under or equal to 10%. It can again be observed that the network ensemble achieves the best results, with 0% error for the training and validation sets and 1.25% error for the testing set samples.

Table 4. Network performance of training, validation and testing sets (in MCCRE [%]) of networks trained with data from the numerical investigation.

Network	'1'	'2'	'3'	'4'	Avg	Ens
Training performance	0.00	2.92	0.00	7.08	0.42	0.00
Validation performance	5.00	3.75	2.08	7.50	2.10	0.00
Testing performance	7.50	8.75	2.50	10.00	2.50	1.25

To study the influence of noise on the numerical damage identification, Figure 10 illustrates the testing performance of the networks of each of the four noise pollution levels. From the figure it can be seen that for data of 1% noise pollution, all networks correctly identify all joint conditions. While some individual networks produce some errors for 2% and 5% noise polluted data, the network ensemble again gives correct damage predictions. It is noted that the network trained with data from measurement location '3' also achieves accurate identifications for 2% and 5% noise pollution. Overall, however, the network ensemble gives the best results - better than the individual location networks and the averaged network. These outcomes highlight the superiority of the network ensemble technique against the approach of simply averaging FRF data from different measurement locations. Further, it demonstrates the efficiency of the

ensemble approach, which filters poor results from underperforming networks and gives outcomes that are at least as accurate as the best performing individual network.

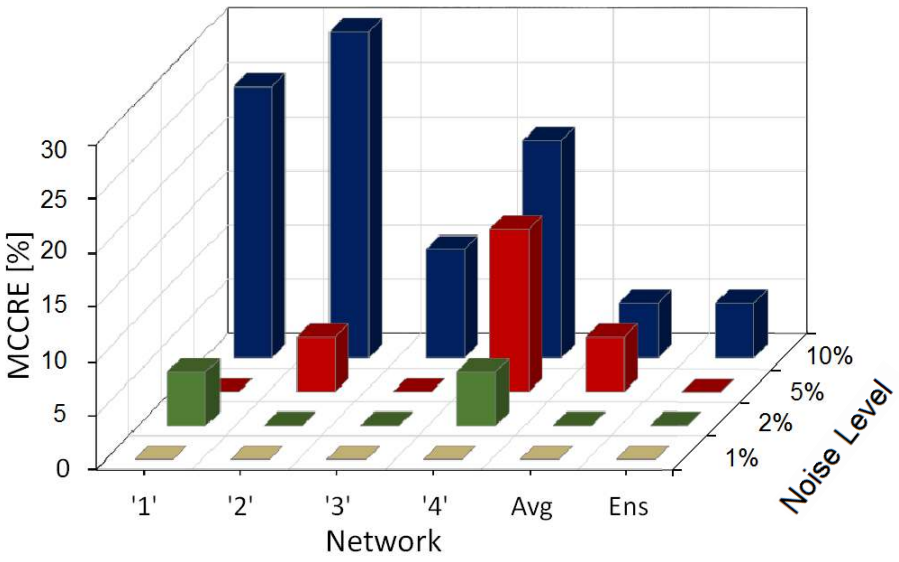

Figure 10. Network performance of testing data set of the numerical investigation subdivided by noise pollution levels.

Summary and conclusions

This paper presented a response-only damage identification method that uses cepstrum analysis for the regeneration of frequency response functions (FRFs) and artificial neural networks (ANNs) for the subsequent identification of joint damage in a multi-storey framed structure with a single input (base excitation).

The proposed method was demonstrated on an experimental and a finite element (FE) model of a two-storey framed structure. Cepstrum analysis was applied to ambient vibration measurements to achieve source-path separation and to generate response-only FRFs. From these, residual FRFs were determined, which represent the difference in FRF data between the undamaged and the damaged structure. Principal component analysis (PCA) techniques were

employed to extract damage features from residual FRFs and to compress large-size FRF data to make them suitable for neural network training. Embedded damage patterns in the FRFs were extracted using a hierarchical system of network ensembles to identify different joint damage cases in the structure. In the network ensemble, first, a number of individual networks were trained with data separated by measurement location, and then the outcomes of the individual networks were fused in the network ensemble to give final damage predictions.

For the experimental investigation, two structural states were tested - in one state, the structure was inflicted with joint damage only, while in the other state, in addition to the joint damage, the structure was also subjected to column damage. This was done to generate data from two testing objects that are structurally similar but not the same. The two unrelated data sets were subsequently used for separate network training and testing in order to provide generalised validation of the proposed method. For the FE study, white Gaussian noise of up to 10% noise-to-signal ratio was added to the numerically generated ambient vibration measurements to simulate field-testing conditions.

The results showed that the proposed method is capable of reliably and accurately identifying joint damage in a multi-storey building/structure based on measured responses to a single input. Recommendations are given as to how this could be applied to the more general multiple-input case. The method has great potential for practical applications as it enables the online monitoring of structures based on response-only measurements in situations where the applied forces are not precisely known.

Acknowledgements

The authors wish to thank the Centre for Built Infrastructure Research (CBIR), Faculty of Engineering and Information Technology, University of Technology Sydney (UTS) for supporting this project. Within the Faculty of Engineering, the authors wish to express their gratitude to the staff of the UTS Structures Laboratory for their assistance in manufacturing the

test structure and for conducting the experimental work using the shake table. Alyuda Research Inc. is gratefully acknowledged for providing a free copy of their Alyuda NeuroIntelligence software.

Funding

The section on cepstrum-based operational modal analysis was supported in part by the Australian Research Council, through Linkage Project [LP110200738].

References

1. Doebling SW, Farrar CR, Prime MB and Shevitz DW. Damage identification and health monitoring of structural and mechanical systems from changes in their vibration characteristics: A literature review. Los Alamos, NM, US: Los Alamos National Laboratory Report LA-13070-MS, 1996.
2. Chang PC, Flatau A and Liu SC. Review paper: Health monitoring of civil infrastructure. Struct Health Monit 2003; 2(3): 257-267.
3. Fan W and Qiao P. Vibration-based damage identification methods: A review and comparative study. Struct Health Monit 2011; 10(1): 83-111.
4. Peeters B, Maeck J and De Roeck G. Vibration-based damage detection in civil engineering: excitation sources and temperature effects. Smart Mater Struct 2001; 10(3): 518-527.
5. Minh-Nghi T, Lardiès J and Marc B. Natural frequencies and modal damping ratios identification of civil structures from ambient vibration data. Shock Vibration 2006; 13(4): 429-444.
6. Ramos LF, Aguilar R and Lourenço PB. Operational modal analysis of historical constructions using commercial wireless platforms. Struct Health Monit 2011; 10(5): 511-521.

7. Devriendt C, De Sitter G, Vanlanduit S and Guillaume P. Operational modal analysis in the presence of harmonic excitations by the use of transmissibility measurements. Mech Syst Signal Process 2009; 23(3): 621-635.
8. Bogert BP, Healy MJR and Tukey JW. The quefrency alanysis of time series for echoes: Cepstrum pseudo-autocovariance, cross-cepstrum and saphe cracking. In: Rosenblatt M (ed) *Time series analysis*. Wiley, New York, 1963, pp. 209-243.
9. Oppenheim AV and Schafer RW. From frequency to quefrency: A history of the cepstrum. IEEE Signal Process Mag 2004; 21: 95-106.
10. Oppenheim AV and Schafer RW. Homomorphic analysis of speech. IEEE Trans Audio Electroacoust 1968; AU-16(2): 221-226.
11. Gao Y and Randall RB. Determination of frequency response functions from response measurements - II. Regeneration of frequency response functions from poles and zeros. Mech Syst Signal Process 1996; 10(3): 319-340.
12. Gao Y and Randall RB. Determination of frequency response functions from response measurements - I. Extraction of poles and zeros from response cepstra. Mech Syst Signal Process 1996; 10(3): 293-317.
13. Randall RB and Gao Y. Extraction of modal parameters from the response power cepstrum. J Sound Vib 1994; 176(2): 179-193.
14. Hanson D, Randall RB, Antoni J, Thompson DJ, Waters TP and Ford RAJ. Cyclostationarity and the cepstrum for operational modal analysis of MIMO systems - Part I: Modal parameter identification. Mech Syst Signal Process 2008; 21: 2441-2458.
15. Hanson D, Randall RB, Antoni J, Thompson DJ, Waters TP and Ford RAJ. Cyclostationarity and the cepstrum for operational modal analysis of MIMO systems - Part II: Obtaining scaled mode shapes through finite element model updating. Mech Syst Signal Process 2008; 21: 2459-2473.

16. Choudhury AR and He J. Structural damage location using expanded measured frequency response function data. In: *Proceedings of the 14th Internatioinal Modal Analysis Conferrence*; Dearborn, Michigan, USA, 1996, pp. 934-942.
17. Sampaio RPC, Maia NMM and Silva JMM. Damage detection using the frequency-response-function curvature method. J Sound Vib 1999; 226(5): 1029-1042.
18. Pandey AK, Biswas M and Samman MM. Damage detection from changes in curvature mode shapes. J Sound Vib 1991; 145(2): 321-332.
19. Ni YQ, Zhou XT and Ko JM. Experimental investigation of seismic damage identification using PCA-compressed frequency response functions and neural networks. J Sound Vib 2006; 290(1-2): 242-263.
20. Dackermann U, Li J and Samali B. Identification of member connectivity and mass changes on a two-storey framed structure using frequency response functions and artificial neural networks. J Sound Vib 2013; 332(16): 3636-3653.
21. Samali B, Dackermann U and Li J. Location and severity identification of notch-type damage in a two-storey framed structure utilising frequency response functions and artificial neural networks. Adv Struct Eng 2012; 15(5): 743-757.
22. Dackermann U, Smith WA and Randall RB. Application of cepstrum analysis and artificial neural networks for the damage identification of a two-storey framed structure based on response-only measurements. In: *Proceedings of the 6th International Conference on Structural Health Monitoring of Intelligent Infrastructure*; Hong Kong, Hong Kong, 2013.
23. Reynders E. System identification methods for (operational) modal analysis: Review and comparison. Arch Comput Meth Eng 2012; 19: 51-124.
24. Peeters B and De Roeck G. Stochastic system identification for operational modal analysis: A review. J Dyn Syst Meas Contr 2001; 123: 659-667.

25. Childers DG, Skinner DP and Kemerait RC. The cepstrum: A guide to processing. Proc IEEE 1977; 65(10): 1428-1443.
26. Randall RB. Vibration-based condition monitoring: Industrial, aerospace and automotive applications. 1th ed. West Sussex, United Kingdom: John Wiley & Sons, Ltd., 2011.
27. Oppenheim AV and Schafer RW. Discrete-time signal processing. 3rd ed. Upper Saddle River, NJ, USA: Pearson Higher Education, 2010.
28. Randall R, Smith W. Cepstrum-based operational modal analysis: Regeneration of frequency response functions, In: *Proceedings of the 7th Australasian Congress on Applied Mechanics*, Adelaide, Australia, 2012, pp. 181-190.
29. Pearson K. On lines and planes of closest fit to systems of points in space. Philos Mag 1901; 2(6): 559-572.
30. White PR, Tan MH and Hammond JK. Analysis of the maximum likelihood, total least squares and principal component approaches for frequency response function estimation. J Sound Vib 2006; 290(3-5): 676-689.
31. Alyuda Research Inc. Alyuda NeuroIntelligence. version 2.2, 2006.